



HAL
open science

Defects in CaF₂ caused by long-time irradiation and their response to annealing

Vojtech Vlcek, Jakub Cizek, Jan Drahokoupil, Jan Valenta, Nobuyoshi Miyajima, Roman Skala

► **To cite this version:**

Vojtech Vlcek, Jakub Cizek, Jan Drahokoupil, Jan Valenta, Nobuyoshi Miyajima, et al.. Defects in CaF₂ caused by long-time irradiation and their response to annealing. Philosophical Magazine, 2010, 90 (20), pp.2749-2769. 10.1080/14786431003745385 . hal-00596600

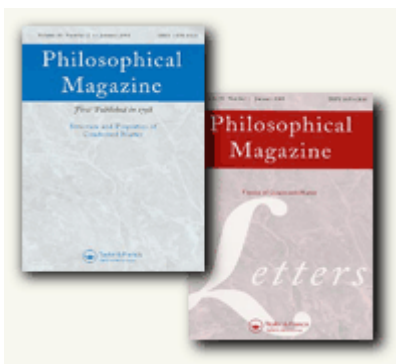
HAL Id: hal-00596600

<https://hal.science/hal-00596600>

Submitted on 28 May 2011

HAL is a multi-disciplinary open access archive for the deposit and dissemination of scientific research documents, whether they are published or not. The documents may come from teaching and research institutions in France or abroad, or from public or private research centers.

L'archive ouverte pluridisciplinaire **HAL**, est destinée au dépôt et à la diffusion de documents scientifiques de niveau recherche, publiés ou non, émanant des établissements d'enseignement et de recherche français ou étrangers, des laboratoires publics ou privés.



Defects in CaF₂ caused by long-time irradiation and their response to annealing

Journal:	<i>Philosophical Magazine & Philosophical Magazine Letters</i>
Manuscript ID:	TPHM-09-Oct-0449.R1
Journal Selection:	Philosophical Magazine
Date Submitted by the Author:	29-Jan-2010
Complete List of Authors:	Vlcek, Vojtech; Bayerisches Geoinstitut; Faculty of Sciences, Institute of Geochemistry, Mineralogy and Mineral Resources Cizek, Jakub; Faculty of Mathematics and Physics Drahokoupil, Jan; Institute of Physics Valenta, Jan; Faculty of Mathematics and Physics Miyajima, Nobuyoshi; Bayerisches Geoinstitut Skala, Roman; Institute of Geology
Keywords:	defects, microstructure, photoluminescence, TEM, X-ray diffraction
Keywords (user supplied):	CaF ₂ , fluorite, PAS



Defects in CaF₂ caused by long-time irradiation and their response to annealing

Vojtěch Vlček^{1,2}, Jakub Čížek³, Jan Drahokoupil^{4,5}, Jan Valenta⁶,
Nobuyoshi Miyajima², Roman Skála^{1,7}

1) Faculty of Sciences, Charles University in Prague, Albertov 6, CZ – 12000, Prague 2, Czech Republic

2) Bayerisches Geoinstitut, Universität Bayreuth, D-95440, Bayreuth, Germany

3) Faculty of Mathematics and Physics, Charles University in Prague, V Holešovičkách 2, CZ-18000, Praha 8, Czech Republic

4) Institute of Physics of the ASCR, v. v. i., Na Slovance 2, CZ-182 21 Prague 8, Czech Republic

5) Faculty of Nuclear Sciences and Physical Engineering, Czech Technical University, Trojanova 13, CZ-120 00, Prague 2, Czech Republic

6) Faculty of Mathematics and Physics, Charles University in Prague, Ke Karlovu 3, CZ-12000, Praha 2, Czech Republic

7) Institute of Geology of the ASCR, v. v. i., Rozvojová 269, CZ-16500 Prague 6, Czech Republic

correspondence author: Vojtěch Vlček vojtech.vlcek@uni-bayreuth.de

Abstract

Samples of CaF₂ irradiated for millions of years in nature were studied by several methods: X-Ray Diffraction, Positron Annihilation Spectroscopy (PAS), Photoluminescence Spectroscopy (PLS), and Transmission Electron Microscopy (TEM). It was shown that the unexpectedly high density of radiation-induced defects present in the fluorite structure (documented by TEM) causes significant micro-strains. Even annealing up to 450 °C cannot completely remove these micro-strains which are stabilised by impurities. The PAS and subsequent theoretical calculations revealed the behaviour of the defects during heating. The PL spectra of irradiated fluorite were interpreted as well.

Keywords: CaF₂, fluorite, microstructure, defects, Positron Annihilation Spectroscopy, Photoluminescence Spectroscopy, Transmission Electron Microscopy, X-ray Diffraction

1 Introduction

Radiation-induced defects in fluorite (CaF₂) structure were investigated only in artificially irradiated samples in the recent studies (e.g., Refs. [1-4]). However, the response of the structure to a long-time irradiation (of the order of million years) is essential for understanding the processes of formation and the stability of defect centres. These recent studies showed that the radiation damage of fluorite should reach a saturation level and then there should be a dynamic balance of creation and

1
2
3 annihilation of the centres resulting in minimum strains within the lattice.

4
5 Understanding how the fluorite structure responds to a long-term irradiation is
6
7 important for its potential use under conditions of prolonged exposition to radiation in
8
9 applications such as containment of radioactive waste (proposed in Ref. [2]), special
10
11 optics or applications in electrotechnics (e.g. Ref. [5]). As a consequence, we chose
12
13 the natural samples of fluorite to evaluate effect of the long-time irradiation on CaF₂
14
15 structure. The microstructure analysis from X-ray powder diffraction data, Positron
16
17 Annihilation Spectroscopy (PAS), Photoluminescence Spectroscopy (PLS) and
18
19 Transmission Electron Microscopy (TEM) were used to decipher the behaviour of
20
21 fluorite under prolonged radiation.
22
23
24
25
26
27
28

29 **2 Experimental methods and sample description**

30 **2.1 Samples**

31
32 A natural CaF₂ sample from Kletno (Poland) was exposed to radiation emitted
33
34 by surrounding uraninite (UO₂) for millions of years. It has a dark purple colour and
35
36 dim surface. This sample was assumed to display the highest degree of irradiation
37
38 damage. Fluorite from Vlastějovice (Czech Republic) was irradiated by allanite (Ce-
39
40 silicate). The activity of this mineral is several times lower in comparison to uraninite.
41
42 Hence, the sample from Vlastějovice was assumed to represent a low-irradiated CaF₂.
43
44 A non-irradiated fluorite sample from the locality Jílové u Děčína (Czech Republic)
45
46 and a synthetic standard (Suprapur, Merck) were used as reference materials.
47
48
49
50
51

52 **2.2 X-ray diffraction**

53
54 X-ray powder diffraction patterns were collected with a PANalytical X'Pert
55
56 Pro diffractometer equipped with an X'Celerator position-sensitive detector and a
57
58 secondary graphite monochromator (Institute of Physics, Academy of Sciences of the
59
60 Czech Republic). Data were step-scanned over the range from 10° to 150° 2 θ with

0.05° step size and 300 s counting time per step. Cobalt tube was operated at 40 kV voltage and 30 mA current.

The naturally irradiated fluorite sample from Kletno annealed up to 450 °C was subsequently X-ray irradiated on conventional X-ray source MIKROMETA (Faculty of Science, Charles University in Prague) with unfiltered radiation from Cu tube operated at 40 kV and 30mA.

The diffraction peak parameters were fitted using Rietveld refinement procedure with Le-Bail fit as implemented in the HighScore software (PANalytical). The Williamson-Hall plot (described in Ref. [6]) is used to visualize the difference between crystallite size and a micro-strain peak broadening.

2.3 PAS

A $^{22}\text{Na}_2\text{CO}_3$ positron source with activity of 1.5 MBq deposited on a 2 μm thick mylar foil was used in PAS measurements. The source was placed in the centre of a small cylindrical chamber with a diameter of 10 mm and height of 5 mm. Subsequently, the chamber was completely filled with the sample powder and closed. Dimensions of the chamber ensure that virtually all positrons are stopped inside the chamber and, thereby, annihilate in the studied powder.

Positron-lifetime measurements were performed on a digital spectrometer described in Refs. [7,8]. The spectrometer is equipped with BaF_2 scintillators and fast photomultipliers Hamamatsu H3378. Detector pulses are directly digitized using a couple of 8-bit ultra-fast digitizers Acqiris DC 211 with sampling frequency of 4 GHz. Analysis of digitized pulses and construction of positron-lifetime spectrum is performed off-line using so called integral true constant fraction technique described in Ref. [9]. The spectrometer exhibits excellent time resolution of 145 ps (full width at half-maximum (FWHM) ^{22}Na). At least 10^7 positron annihilation events were

1
2
3 accumulated in each positron lifetime spectrum. Decomposition of positron-lifetime
4 spectra into exponential components were performed using a maximum likelihood
5 procedure described in Ref. [10]. The source contribution to positron-lifetime spectra
6 consisted of two weak components with lifetimes of ~ 368 ps and ~ 1.5 ns and
7 corresponding intensities of ~ 8 % and ~ 1 %. These components represent a
8 contribution of positrons annihilated directly in Na_2CO_3 source and the covering
9 mylar foils.
10
11
12
13
14
15
16
17
18
19

20 Coincidence Doppler broadening (CDB) studies were carried out using a
21 spectrometer [11] equipped with two high purity Ge detectors. The overall energy
22 resolution of the CDB spectrometer is (1.02 ± 0.01) keV at 511 keV. At least 10^8
23 annihilation events were collected in each of two-dimensional γ -ray energy spectra,
24 which were subsequently reduced into two one-dimensional cuts representing the
25 resolution function of spectrometer and Doppler broadened annihilation profile. In
26 this paper CDB results are presented as ratio curves with respect to a well annealed
27 bulk Mg (99.99 %) reference specimen
28
29
30
31
32
33
34
35
36
37
38

39 Theoretical calculations of positron parameters were performed from the first
40 principles using an approach based on the density functional theory. Positron wave
41 function was calculated within so-called conventional scheme employing the atomic
42 superposition (ATSUP) method [12]. Electron-positron correlation was treated within
43 local density approximation (LDA) using the scheme developed by Boronski and
44 Nieminen [13] with the correction [14] for incomplete positron screening with high
45 frequency dielectric constants $\epsilon_\infty = 6.8$ [15]. A cubic structure with lattice parameter a
46 = 5.46305 Å [16] was adopted for CaF_2 . A supercell approach was used for
47 calculations of positron parameters for CaF_2 crystal containing defects. The
48 calculations were performed on 768 atom-based supercells. Vacancies or vacancy
49
50
51
52
53
54
55
56
57
58
59
60

1
2
3
4 agglomerates were created simply by removing the appropriate number of atoms from
5
6 the supercell.

7
8 The high momentum part (HMP) of momentum distribution of electrons that
9
10 annihilated positrons was performed using ATSUP-based approach according to the
11
12 scheme described in Refs. [17,18]. Electron-positron correlation was treated using
13
14 LDA approach [13,14] and also by generalized gradient approximation (GGA)
15
16 scheme developed by Barbiellini et al. [19,20]. Only the contribution from positrons
17
18 annihilated by localized core electrons were considered in the calculations. Hence,
19
20 comparison of calculated HMP curves with experiment is meaningful only in the high
21
22 momentum range, $p > (10 \times 10^{-3}) m_{oc}$, where contribution of positrons annihilated by
23
24 core electrons dominates. The following orbitals were considered as core electrons
25
26 and included in the calculations of HMP curves: Ca: $1s^2, 2s^2, 2p^6, 3s^2, 3p^6$, F:
27
28 $1s^2, 2s^2, 2p^5$, Mg: $1s^2, 2s^2, 2p^6$.

29
30
31
32
33
34 The final one-dimensional HMP curve, which can be compared to the
35
36 experimental CDB spectrum is obtained by summing up the contributions of the core
37
38 states of all atoms in the system and integrating over the high-momentum tail. In
39
40 order to compare the calculated HMP curves to experimental CDB spectra, they have
41
42 to be properly normalized. The areas of the experimental CDB spectra were scaled to
43
44 unity, while the areas below the theoretical HMP curves were set equal to λ_{core} / λ ,
45
46 where λ_{core} is the annihilation rate with all core electrons of the system, while λ is the
47
48 total annihilation rate, i.e. the inverse of positron lifetime. In order to mimic the effect
49
50 of the finite resolution of the experimental setup, the theoretical HMP curves were
51
52 convoluted with a Gaussian with FWHM of $(4.0 \times 10^{-3}) m_{oc}$.
53
54
55
56
57
58
59
60

2.4 PLS

The high- and low-irradiated fluorite and the reference sample of synthetic CaF_2 were investigated by photoluminescence micro-spectroscopy. In addition to that also the high-irradiated sample annealed to 450 °C was investigated after exposure to X-rays. The PL emission was collected by the inverted microscope Olympus IX-71 with 20x magnification objective lens and detected with the liquid-nitrogen cooled BI-CCD camera attached to the imaging spectrometer Acton SpectraPro 2150i. The data were measured at room temperature. PL was excited by a diode laser emitting at 405 nm. Several measurements were made on different positions of each sample in order to obtain reasonable statistics. The data were fitted by Fityk software [21] using split Gaussian function, which refines peak half-widths separately.

2.5 TEM

Powdered fluorite samples (from Kletno, Vlastějovice and synthetic CaF_2) were placed onto TEM copper grids coated with carbon holey films. Microscope used to study the samples was a Philips CM 20 FEG (at the Bayerisches Geoinstitut, Universität Bayreuth, Germany) operated at 200 kV voltage. The samples were imaged under bright field, dark field, and weak-beam dark-field conditions. Also, high-resolution TEM images were acquired. Selected area electron diffraction was used to define orientation of the samples. In order to investigate existence of some impurities, energy-dispersive X-ray spectra were also collected with 60 sec live time.

3 Results and discussion

3.1 X-ray diffraction

The diffraction peaks of the irradiated sample are broadened mainly due to micro-strain that is caused by defects and lattice deformations; the domain size broadening has negligible contribution. The diffraction patterns were collected during in-situ heating at different temperatures to obtain information about the structure

1
2
3 recovery caused by annealing. Subsequent peak-broadening analysis using
4
5 Williamson-Hall method [6] confirmed the expected decrease of micro-strain values.
6
7
8 The data plotted in Williamson-Hall graph (Fig. 1) shows that the main recovery
9
10 process is started at temperatures higher than 300 °C. To determine possible slow
11
12 kinetics at lower temperature the several measurements were done at 300 °C (total
13
14 heating lasted 8 hours), however no change of micro-strain was observed.
15
16

17
18 The annealed sample (up to 450 °C) became colourless after the experiment,
19
20 yet some micro-strains remained. We assume that some defects persist and are not
21
22 affected by heating. It should be noted that the reference samples from Jílové and the
23
24 synthetic CaF₂ showed also non-zero values of micro-strain. Nevertheless, these
25
26 micro-strain values are substantially lower than those observed in the annealed and X-
27
28 ray irradiated samples.
29
30

31
32 Another interesting feature noted in the annealed samples is a colour change
33
34 from colourless to purple upon irradiation by the X-ray beam during the XRD study.
35
36 The stability of colouration depends on the time of X-ray irradiation. After a short
37
38 irradiation (about 1 hour) the colour dissipates in about three days; however after
39
40 irradiation that took more than 500 hours the colour is stable. X-ray irradiation does
41
42 not affect the microstructure characteristics of the sample (no peak-broadening was
43
44 observable in diffraction pattern). This confirms the different character of the colour
45
46 centers and the defects causing microdeformation.
47
48
49
50

51 52 **3.2 PAS**

53 54 *3.2.1 Theoretical calculations*

55
56 First principles calculations of positron characteristics were performed in
57
58 order to identify defects in CaF₂ samples. Table 1 shows calculated positron lifetimes
59
60 for various positron states in CaF₂ crystal. Calculated positron density in (110) plane

1
2
3 for a perfect defect-free CaF_2 crystal is plotted in Fig. 2 A. Positron in a perfect CaF_2
4 crystal is delocalized in the lattice in the form of modulated Bloch-like wave.
5
6

7
8 Calculated bulk positron lifetime in a perfect CaF_2 crystal is 171.5 ps.
9

10 Figure 2 B shows calculated positron density in CaF_2 containing an F-
11 vacancy. Although there is a slight enhancement of positron density in the vicinity of
12 F-vacancy, there is still a significant probability to find positron elsewhere. Hence, F-
13 vacancy is too shallow trap incapable to confine positron. This is confirmed by
14
15 F-vacancy is too shallow trap incapable to confine positron. This is confirmed by
16
17 positron lifetime, which approaches the bulk positron lifetime in CaF_2 and also by a
18
19 negligible positron binding energy to F-vacancy, see Table 1.
20
21
22
23

24 On the other hand, Ca-vacancy is a deep positron trap. Fig. 2 C shows that
25
26 positron is completely localized in Ca-vacancy. Calculated lifetime of positron
27
28 trapped in Ca-vacancy is 225.9 ps and positron binding energy to this defect is 1.68
29
30 eV.
31
32

33
34 Thus, theoretical calculations clearly demonstrated that F-vacancies as very
35
36 shallow traps are “invisible” to positrons. On the other hand, Ca-vacancies as strong
37
38 traps can be undoubtedly detected by PAS.
39
40

41 It is known that F-vacancies produced in CaF_2 by irradiation aggregate and
42
43 form fluorine voids [22-25]. This process leads to formation of metallic Ca inclusions
44
45 in CaF_2 where fluorine voids occur and only Ca atoms remain in their sites. Due to
46
47 this reason, it is important to examine the possibility of positron trapping in
48
49 aggregates of F-vacancies. Figure 3 shows results of the first principle calculations of
50
51 positron parameters for F-vacancy aggregates of various sizes. One can see in Fig. 2
52
53 that positron lifetime and positron binding energy to an aggregate of F-vacancies
54
55 increases with increasing number of F-vacancies (i.e., increasing size of fluorine
56
57 void). The calculated positron density for a CaF_2 crystal containing F-divacancy is
58
59
60

1
2
3 plotted in Fig. 4 A. Similarly to F-vacancy also F-divacancy is too shallow trap to
4
5 confine positron. This is demonstrated not only by absence of positron localization,
6
7 but also by calculated positron lifetime, which is close the bulk positron lifetime in
8
9 perfect CaF₂ and very small positron binding energy to F-divacancy.
10
11

12
13 A remarkable increase of positron binding energy occurs for F-tetravacancy,
14
15 see Fig. 3 B. Calculated positron density for a CaF₂ crystal containing F-tetravacancy
16
17 is plotted in Fig. 4 B and shows a significant increase of positron localization. Hence,
18
19 F-tetravacancy becomes capable of positron trapping and can be detected by PAS.
20
21 Even larger aggregates of F-vacancies are yet deeper traps characterized by a longer
22
23 positron lifetime and higher positron binding energy, (Fig. 3). Figure 5 A shows
24
25 calculated positron density for an agglomerate of 8 F-vacancies. One can see that
26
27 positron is fully localized and lifetime of positrons trapped at this defect is
28
29 comparable to that of positron trapped in Ca-vacancy (Fig. 3 A).
30
31
32
33

34
35 Calculated positron characteristics for a CaF₂ supercell with all F atoms
36
37 removed represents an extreme case and simulates a very large fluorine void; it is
38
39 plotted in Fig. 5 B. The figure illustrates that positron is delocalized inside the
40
41 fluorine void and is located mostly in the empty sites in fluorine sub-lattice. Lifetime
42
43 of positron delocalized in very large fluorine void is 301.9 ps and positron binding
44
45 energy is 1.44 eV.
46
47
48

49 3.2.2 Positron lifetime spectroscopy

50
51 The reference non-irradiated CaF₂ powder exhibits a two-component positron
52
53 lifetime spectrum. The shorter component with lifetime $\tau_1 = (110 \pm 10)$ ps and relative
54
55 intensity $I_1 = (41 \pm 1)$ % can be attributed to free, delocalized positrons. The longer
56
57 component with lifetime $\tau_2 = (322 \pm 2)$ ps and relative intensity $I_2 = (59 \pm 1)$ % is a
58
59 contribution of positrons trapped at defects. The lifetime τ_2 of this component is
60

longer than lifetimes calculated for aggregates of F-vacancies (Fig. 3 A). It is even longer than the upper limit for F-vacancy aggregates, i.e., positron lifetime of 302 ps calculated for a large fluorine void. Hence, the longer component in positron lifetime spectrum of reference CaF₂ powder represents a contribution of positrons trapped at larger defects (voids) containing not only F-vacancies, but also Ca-vacancies.

In the frame of the two-state **simple trapping model** [26] the quantity

$$\tau_f = \left(\frac{I_1}{\tau_1} + \frac{I_2}{\tau_2} \right)^{-1} \quad (1)$$

equals to the bulk positron lifetime

$$\tau_f \equiv \tau_B \quad (2)$$

Equations (1,2) are frequently used to check the consistency of spectrum decomposition with the two-state **simple trapping model**. For the reference CaF₂ powder we obtained $\tau_f = (179 \pm 8)$ ps, which is in a good agreement with the calculated bulk positron lifetime in a perfect CaF₂ crystal shown in Table 1. This confirms that assumptions of two-state **simple trapping model** (i.e., a single type of uniformly distributed defects) are fulfilled in the case of virgin CaF₂ powder. **Note that positron annihilations studies of CaF₂ crystals were performed by angular-correlation [27] but no positron lifetime investigations of CaF₂ crystals have been performed so far to our best knowledge.**

The irradiated natural CaF₂ powder from Kletno exhibits two-component positron lifetime spectrum. Both lifetimes τ_1 , τ_2 of these components are longer than the bulk positron lifetime in CaF₂. Thus, both these components represent a contribution of positrons trapped at defects. The longer component exhibits lifetime $\tau_2 = (335 \pm 4)$ ps, which is comparable with the lifetime τ_2 measured on the reference powder. Hence, similarly to the reference powder, the longer component in **the** irradiated CaF₂ can be attributed to positrons trapped at larger voids containing both

1
2
3 F-vacancies and Ca-vacancies. On the other hand, the shorter component with lifetime
4
5 $\tau_1 = (197 \pm 1)$ ps represents a contribution of positrons trapped at new defects created
6
7 by irradiation. It is well known that agglomerates of F-vacancies are formed in
8
9 irradiated CaF₂ [22-25]. Indeed, the lifetime τ_1 corresponds to the calculated lifetime
10
11 of positrons trapped at an agglomerate of 4 F-vacancies (Fig. 3 A).
12
13

14
15 The irradiated CaF₂ powder from Kletno was subsequently subjected to
16
17 isochronal annealing. The mean positron lifetime is
18

$$19 \tau_{mean} = \sum_i I_i \tau_i, \quad (3)$$

20
21 where the centre of mass of positron-lifetime spectrum is a robust single
22
23 parameter, which is not influenced by mutual correlations of fitted parameters. Figure
24
25 6 shows dependence of the mean positron lifetime on the annealing temperature for
26
27 irradiated CaF₂ powder from Kletno. There is a strong increase of τ_{mean} in the
28
29 temperature range from 200 to 300°C indicating a change of defect structure. Finally,
30
31 above 300°C, the mean lifetime decreases.
32
33
34
35

36
37 More information can be obtained from decomposition of positron lifetime
38
39 spectra. At all annealing temperatures positron-lifetime spectra of irradiated CaF₂ are
40
41 well fitted by two components. Lifetimes of these two components are plotted in Fig.
42
43 7 A as a function of annealing temperature whereas Fig. 7 B shows temperature
44
45 dependence of the intensity I_2 of the longer component.
46
47
48

49 Lifetime τ_1 of positrons trapped at F-vacancy agglomerates gradually
50
51 increases with annealing temperature (inset in Fig. 7 A) indicating increasing size of
52
53 the agglomerates. The intensity I_1 of positrons trapped at F-vacancy agglomerates
54
55 plotted in Fig. 7 B increases remarkably after annealing above 300°C. This behaviour
56
57 indicates that agglomeration of irradiation-induced single F-vacancies or very small
58
59 F-vacancy clusters occurs at temperatures $T \geq 300^\circ\text{C}$. Theoretical calculations in
60

1
2
3 section 3.2.1 demonstrated that isolated F-vacancies or very small F-vacancy
4
5 agglomerates containing less than 4 F-vacancies cannot be detected by PAS.
6
7
8 However, larger agglomerates containing at least 4 F-vacancies are capable of
9
10 positron trapping and can be detected by PAS. Hence, agglomeration of isolated F-
11
12 vacancies or very small F-vacancy clusters into larger agglomerates, which takes
13
14 place at temperatures $T \geq 300^\circ\text{C}$, enhances positron trapping to these defects, which is
15
16 reflected by an increase of intensity I_1 . This is accompanied by a gradual increase of
17
18 lifetime τ_1 of this component due to increasing average size of F-vacancy
19
20 agglomerates. The lifetime τ_2 of the longer component increases after annealing at
21
22 300°C . This could be due to F interstitials (*H*-centres) which become mobile at 300°C
23
24 and form fluorine bubble-like defects (described e.g. in Ref. [22]) in the sample.
25
26
27 Positrons trapped at these fluorine bubbles contribute to the longer component and
28
29 causes an increase of lifetime τ_2 .
30
31
32
33
34

35 3.2.3 Coincidence Doppler Broadening

36
37 Figure 8 shows calculated HMP profiles for a perfect CaF_2 crystal and
38
39 reference defect-free pure Mg. The experimental curves for a reference non-irradiated
40
41 CaF_2 powder and a well annealed bulk Mg are plotted in the figure as well. It is clear
42
43 that the curves calculated using GGA scheme are in better agreement with experiment
44
45 than curves calculated using LDA approach. This is due to well known fact that LDA
46
47 overestimates positron annihilations with core electrons [21]. Due to this reason only
48
49 the curves calculated using GGA scheme will be considered in the further discussion.
50
51
52 As was explained in section 3.2.1, only localized core electrons which retain their
53
54 atomic character are considered in the calculations of HMP profiles. Low momentum
55
56 valence electrons were not included in the calculations. Therefore, comparison of
57
58
59
60 calculated curves with experiment is meaningful only in the high momentum range p

1
2
3 $> 10 \times 10^{-3} m_0c$, where positron annihilations with localized core electrons dominate.
4
5
6 Indeed, one can see in Fig. 8 that experimental curves for reference CaF_2 and Mg are
7
8 well reproduced by theoretical calculations in the high momentum range $p > 10 \times 10^{-3}$
9
10 m_0c .

11
12
13 The contributions of various electron orbitals to the calculated HMP profile
14
15 for a perfect CaF_2 crystal are plotted in Fig. 9. From comparison of experimental
16
17 profile with theoretical calculations, it is clear that positrons are annihilated mostly by
18
19 F electrons. This is not surprising because there is an attractive Coulomb interaction
20
21 between positron and F anions. Thus, in a perfect CaF_2 crystal the overlap of positron
22
23 density with F anions is significantly larger than with Ca cations, see Fig. 2 A.
24
25

26
27 Figure 10 shows the ratio curve (related to Mg reference) for the reference
28
29 non-irradiated CaF_2 powder and naturally irradiated CaF_2 sample from Kletno in the
30
31 as-received state and after annealing to various temperatures. The ratio curves exhibit
32
33 a sharp peak located at $p \sim (9 \times 10^{-3}) m_0c$. This is mainly due to contribution of
34
35 positrons annihilated by fluorine $2p$ electrons. The second important feature is a broad
36
37 peak at $p \sim (40 \times 10^{-3}) m_0c$, which represents a contribution of positrons annihilated
38
39 by fluorine s -electrons.
40
41
42

43
44 The irradiated CaF_2 sample is characterized by a decrease in amplitudes of
45
46 both peaks in the ratio curves (Fig. 10). This confirms that the contribution of
47
48 positrons annihilated by fluorine electrons is reduced in the irradiated sample. This is
49
50 in accordance with formation of F-vacancy aggregates detected by positron-lifetime
51
52 spectroscopy. Contrary to free positrons delocalized in perfect CaF_2 crystal, positrons
53
54 localized in F-vacancy aggregates (containing at least 4 F-vacancies) are annihilated
55
56 mostly by Ca-electrons because fluorine atoms are missing in F-vacancy aggregates.
57
58
59
60

1
2
3 Hence, an increase in positron trapping in F-vacancy aggregates causes a decrease in
4
5 fraction of positrons annihilated by F-electrons.
6
7

8 This effect can be seen also on the calculated HMP curves plotted in Fig. 11.
9
10 Clearly, the calculated ratio curves for positrons trapped at F-vacancy agglomerates
11
12 are lower than the curve for a perfect CaF_2 crystal. This is due to reduced contribution
13
14 of positrons annihilated by F-electrons. The ratio curve for F-vacancy agglomerate
15
16 containing 8 F-vacancies is located below the curve for agglomerate containing 4
17
18 vacancies because the contribution of positrons annihilated by F-electrons decreases
19
20 with increasing size of the agglomerate.
21
22
23

24 On the other hand, the calculated ratio curve for positrons trapped in Ca-
25
26 vacancy is situated above the curve for a perfect CaF_2 because F-atoms occupy the
27
28 nearest neighbour sites of Ca-vacancy. Hence, there is relatively high probability that
29
30 it will be annihilated by F-electron, while the probability to be annihilated by Ca-
31
32 electron is negligible.
33
34
35

36 With increasing temperature the fraction of positrons annihilated by F-
37
38 electrons firstly decreases due to increasing size of F-vacancy agglomerates (Fig. 10
39
40 B). The lowest contribution of the positrons annihilated by F-electrons was found
41
42 after annealing at 100°C . Annealing to temperatures above 200°C leads to an increase
43
44 of fraction of positrons annihilated by F-electrons because positrons become trapped
45
46 at fluorine bubbles, i.e., the fraction of positrons annihilated by F-electrons increases.
47
48 This enhancement of fraction of positrons annihilated by F-electrons agrees with
49
50 increase of lifetime τ_2 observed by positron-lifetime spectroscopy (Fig. 7 A) and
51
52 explained by formation of fluorine bubbles.
53
54
55
56
57
58
59
60

3.3 PLS

The detected PL spectra revealed a distinct behaviour of irradiated and non-irradiated fluorites. Six different emission bands with peaks at about 431, 479, 514, 587, 644, and 720 nm were observed. They are labelled E_1 to E_6 , respectively, and they are listed in Table 3. However the natural reference fluorite sample from Jílové shows no emission bands, this confirms absence of impurities or luminescent defects. The E_2 and E_5 bands are present in the synthetic reference sample and some irradiated samples and seem to be unaffected by heating or X-ray irradiation. Therefore these bands cannot be related to radiation-induced defects. We assigned the E_2 emission peak (corresponding to 2.59 eV) to oxygen centres (e.g. Ref. [28]).

For the irradiated samples the E_1 , E_3 and E_6 emission bands are characteristic (Fig. 12). The first one has the highest intensity and low FWHM (i.e., narrow energy distribution). It corresponds to energy of 2.88 eV and it is not affected by the annealing or further X-ray irradiation. The E_3 is a broad emission peak corresponding to energy of 2.41 eV. Its position is not affected by the annealing. The E_6 has a broad FWHM and its centre corresponds to energy of 1.72 eV. This emission is not present in the annealed samples which became colourless upon annealing but the E_6 emission reappears again in the samples irradiated by X-ray after being annealed.

The E_1 emission band can be assigned either to F -centres or their clusters or to the impurities, which cause emissions slightly shifted to lower wavelengths. This effect is discussed in previous studies for, e.g., Zn^+ , see [4], or Eu^{2+} , see [29] Since impurities are common in all natural samples both impurities and F -centers can be expected to contribute to the E_1 emission band. Defect centres in natural samples could be bound to the foreign atoms in the structure. This binding makes the defects more stable and resistant to heating. However, the exact character of the substituents is difficult to identify as even very low concentration (ppm) can cause the luminescent

1
2
3 effect and an additional study would be necessary to get the desired information. As
4
5 the E_3 emission has behaviour similar to E_1 it probably represents the same type of
6
7 luminescence centres. The interpretation of the E_6 emission band seems to be more
8
9 complicated as it is influenced by heating and X-ray irradiation; it will be discussed
10
11 later.
12
13

14
15 In the annealed samples the additional E_4 emission appears; corresponds to
16
17 energy of 2.11 eV. However, it is placed in the region of a broad absorption band of
18
19 F - or H -centres, see [4]. We suppose that the E_4 emission is present in irradiated
20
21 sample before heating but it is absorbed within the sample. The small emission bands
22
23 of different peak shape and very low FWHM visible on Figure 12 B are most likely
24
25 emissions of impurities. As they should not be affected by heating, their presence only
26
27 in the spectrum of annealed CaF_2 indicates that the (F and H -centers) absorption band
28
29 disappeared.
30
31
32

33
34 The annealed samples of fluorite when X-ray irradiated exhibit the same PL
35
36 spectra as untreated samples. As the XRD results showed that no new structural
37
38 defects are formed (described in section 3.1) we assume that the E_6 emission is
39
40 connected with some centres, which cannot be detected by XRD. The F -centers,
41
42 which are known to be present in the irradiated CaF_2 samples, are considered as most
43
44 probable candidates. Hence, one should take into account thermal stability of F -
45
46 centres. Most probably electron is released from F -centre during heating and the
47
48 following X-ray irradiation causes the electron trapping again. It is in agreement with
49
50 the observation that the reference non-irradiated material, which does not contain F -
51
52 centres, does not change its colour in X-ray beam. These processes (electron releasing
53
54 and trapping) can also explain the E_6 emission band and its disappearance due to
55
56 annealing.
57
58
59
60

3.4 TEM

Samples of high- and low-irradiated fluorite and the reference sample of synthetic CaF_2 were investigated by TEM. The TEM-EDS analysis showed no mutual intersample chemical differences within the instrument limits. Increasing defect concentration depending on radiation source activity was observed. The reference material showed no defects observable by TEM. However, in the low irradiated samples from Vlastějovice the dislocation loops are documented (Fig. 13 A). It is in a good agreement with results of previous studies [3]. The Kletno sample contains unexpectedly high density of defects as illustrated in the weak-beam dark-field image shown in Fig. 13 B. The dislocation density is so high in this case that it makes almost impossible to distinguish individual dislocations or dislocation-loops. The high-resolution TEM image (Fig. 14) also confirms the presence of Ca inclusions, previously reported from irradiated samples, e.g., by [30]. These inclusions are produced by *F*-centres clustering and they represent stable void-superlattice. However, the Ca inclusions are not present in the low-irradiated sample. This is probably due to different activities of radiation source.

4 Conclusions

The present study characterizes CaF_2 structure with a high density of radiation-induced defects created by long-time irradiation (in order of million of years) that causes significant lattice micro-strains whereas some previous studies (e.g. [2]) expected only low lattice strains and consequently also suggested CaF_2 as a candidate for the containment of radioactive waste. These micro-strains decrease rapidly during heating to temperatures exceeding 300 °C. However the domain-size broadening was not observed. It was also shown that even after annealing some defects remain present in the structure (documented by non-zero strain observed by XRD or by PL spectra). The first principles PAS calculations showed that

1
2
3 agglomerates of F-vacancies are detectable by PAS if they contain at least 4 F-
4
5 vacancies. Lifetime of positrons trapped at F-vacancy agglomerates depends on size
6
7 of the agglomerate and falls in the range from 190 to 302 ps. The presented positron
8
9 lifetime spectroscopic study have not been performed so far and substantially helped
10
11 to reveal the character of the defects and their behaviour. The detail measurements
12
13 showed the presence of *F*-centre agglomerates and their clustering during heating as
14
15 well as the *H*-centre clustering creating free fluorine bubbles in the structure. The
16
17 knowledge of these processes on the atomistic scale could be necessary for using
18
19 CaF_2 as a material for high-resolution electron beam lithography or as an insulating
20
21 layer for semiconductor technology as discussed in Ref. [5].
22
23
24
25
26

27 The defect-related emissions in PL spectra of irradiated CaF_2 were discussed
28
29 in previous studies (e.g., [4]) without concrete assignment; as the results obtained
30
31 from other methods revealed the true character of the defects we were able to make
32
33 this assignment. The PL spectra also showed that the resistant defects are most
34
35 probably stabilized by impurities; this kind of defects could then significantly
36
37 influence the quality of optical devices mainly by causing decrease in transmittance.
38
39
40

41 Saturated positron trapping confirms a high-density of defects in irradiated CaF_2 ,
42
43 which was documented also by TEM observations.
44
45
46

47 5 Acknowledgement

48 This work was funded by the The Ministry of Education of The Czech Republic (projects
49 MSM0021620855 and MS0021620834). One of the authors (JV) acknowledges the support through
50 the Centre of nanotechnology and materials for nanoelectronics, LC510 (funded by the MSMT CR).
51 RS thanks for the support through the research plan AV0Z30130516 of the Institute of Geology AS
52 CR.
53
54

55 6 Literature

- 56
57 [1] M. Boccanfuso, A. Benyagoub, M. Toulemonde, C. Trautmann, K. Schwartz, Ch.
58 Dufour, Nucl Instr and Met in Phys Res B 175 – 177 (2001) p. 590 - 593
59 [2] L. T. Chadderton, Radiation Measurements 36 (2003) p. 13 – 34
60 [3] M. Watanabe, T. Noma, K. Yasuda, K. Yasunaga, S. Matsumura, C. Kinoshita,
16th International Microscopy Congress Abstracts (2006)

- 1
2
3
4 [4] X. Xiang, X. T. Zu, S. Zhu, T. H. Ding, L. M. Wang, *Opt Mat* 28 (2006) p. 930 -
5 934
6 [5] T. Kogure, K. Saiki, M. Konno, T. Kamino, *Mat Res Soc Symp Proc Vol* 504
7 (1998) p. 183 - 188
8 [6] H. P. Klug, L. E. Alexander, *X-Ray Diffraction Procedures*, Wiley, New York,
9 2nd edn. 1974
10 [7] F. Bečvář, J. Čížek, I. Procházka, and J. Janotová, *Nucl. Instrum. Methods A* 539
11 (2005) 372
12 [8] F. Bečvář, J. Čížek, and I. Procházka, *Appl. Surf. Sci.* 255 (2008) 111
13 [9] F. Bečvář, *Nucl. Instrum. Methods B* 261 (2007) 871
14 [10] I. Procházka, I. Novotný, and F. Bečvář, *Mater. Sci. Forum* 255-257 (1997) 772
15 [11] J. Čížek, I. Procházka, B. Smola, I. Stulíková, R. Kužel, Z. Matěj, and V.
16 Cherkaska, *Phys. Stat. Sol. (a)* 203 (2006) 466
17 [12] M.J. Puska and R.M. Nieminen, *J. Phys. F: Met. Phys.* 13 (1983) 333
18 [13] E. Boroński, R.M. Nieminen, *Phys. Rev. B* 34 (1986) 3820
19 [14] M.J. Puska, S. Mäkinen, M. Manninen, and R.M. Nieminen *Phys. Rev. B* 39
20 (1989) 7666
21 [15] S.K. Dickinson, *Infrared laser windows materials property data for ZnSe, KCl,*
22 *NaCl, CaF₂, SrF₂, BaF₂*, Air Force Cambridge Res. Lab. Report AFCRL-TR-
23 75-0318 (1975)
24 [16] R. W. G. Wyckoff, *Crystal Structures*, 9th ed., vol. 1, Interscience/John Wiley,
25 New York, 1963
26 [17] M. Alatalo, B. Barbiellini, M. Hakala, H. Kauppinen, T. Korhonen, M. J. Puska,
27 K. Saarinen, P. Hautojärvi, and R. M. Nieminen, *Phys. Rev. B* 54 (1996) 2397
28 [18] J. Kuriplach, A. L. Morales, C. Dauwe, D. Segers, and M. Šob, *Phys. Rev. B* 58
29 (1998) 10475
30 [19] B. Barbiellini, M. J. Puska, T. Torsti, and R. M. Nieminen, *Phys. Rev. B* 51
31 (1995) 7341
32 [20] B. Barbiellini, M. J. Puska, T. Korhonen, A. Harju, T. Torsti, and R. M.
33 Nieminen, *Phys. Rev. B* 53 (1996) 16201
34 [21] M. Wojdyr, *Fityk A curve fitting and data analysis program*, software available
35 at <http://www.unipress.waw.pl/fityk/>
36 [22] E. Johnson, and L. T. Chadderton, *Micron* 2 (1980) 247-250
37 [23] E. Johnson, L.T. Chadderton, *Radiat. Effects* 79 (1983) 183
38 [24] R. Bebbewitz, D. Smith, *Phys. Rev. B* 59 (1999) 8237
39 [25] L. P. Cramer, S. C. Langford, and J. T. Dickinson, *J. Appl. Phys.* 99, 054305
40 (2006)
41 [26] R. West, in *Positrons in Solids*, edited by P. Hautojärvi (Springer-Verlag, Berlin,
42 1979), p. 89.
43 [27] W. Brandt, G. Coussot, Paulin R., *Phys. Rev. Lett.* 23, (1969) p. 522 - 524
44 [28] E. Radzhabov, *J. Phys. Condens. Matter* 6 (1994) p. 9807-9815
45 [29] Z. Hao, J. Cai, L. Yi, *J. Lum.* 40&41 (1988) p. 393 - 394
46 [30] L. T. Chadderton, E. Johnson, T. Wohlenberg, *Physica Scripta Vol.* 13 (1976) p.
47 127 - 128
48
49
50
51
52
53
54
55
56
57
58
59
60

Table 1. Results of the first principles calculations of positron parameters (positron lifetime τ and positron binding energy to defect E_B) for various positron states in CaF_2 .

	τ (ps)	E_B (eV)
bulk	171.5	-
F-vacancy	172.1	0.008
Ca-vacancy	225.9	1.680

For Peer Review Only

Table 2. Results of positron lifetime measurements of CaF₂ powders.

Sample	τ_1 (ps)	I_1 (%)	τ_2 (ps)	I_2 (%)
reference, non-irradiated	110 ± 10	41 ± 1	322 ± 2	59 ± 1
irradiated, Kletno	197 ± 1	67 ± 1	335 ± 4	33 ± 1

For Peer Review Only

Table 3. Observed emission bands and their assignment.

Emission	λ (nm)	Assignment
E ₁	431	F-centres bound to substituent
E ₂	479	non-radiation-induced defects
E ₃	514	F-centres bound to substituent
E ₄	587	F- / H- centres
E ₅	644	non-radiation-induced defects
E ₆	720	electron-defect bound state

For Peer Review Only

1
2
3
4
5
6
7
8
9
10
11
12
13
14
15
16
17
18
19
20
21
22
23
24
25
26
27
28
29
30
31
32
33
34
35
36
37
38
39
40
41
42
43
44
45
46
47
48
49
50
51
52
53
54
55
56
57
58
59
60

For Peer Review Only

Figure captions

Fig. 1 Williamson-Hall plot showing the data obtained through whole powder pattern fitting. The source powder patterns were measured *in-situ* during annealing. The micro-strain is proportional to the slope of the linear regression.

Fig. 2 Calculated positron density in (110) plane for (A) a perfect CaF₂ crystal, (B) CaF₂ crystal containing F-vacancy, and (C) CaF₂ crystal containing Ca-vacancy. Positron density is expressed in atomic units; distances are shown in units of CaF₂ lattice parameter.

Fig. 3 Results of first principle calculations of positron parameters for F-vacancy agglomerates: (A) positron lifetime and (B) positron binding energy as a function of number of F-vacancies in the agglomerate. Dashed lines show positron parameters for a perfect CaF₂ crystal, dash-dotted lines show positron parameters for Ca-vacancy and dotted lines show positron parameters for a large fluorine void.

Fig. 4 Calculated positron density in (110) plane for a CaF₂ crystal containing (A) F-divacancy, (B) F-tetravacancy. Positron density is expressed in atomic units; distances are shown in units of CaF₂ lattice parameter.

Fig. 5 Calculated positron density in (110) plane for a CaF₂ crystal containing (A) an agglomerate of 8 F-vacancies, (b) a large fluorine void. Positron density is expressed in atomic units; distances are shown in units of CaF₂ lattice parameter.

Fig. 6 Temperature dependence of the mean positron lifetime τ_{mean} for naturally irradiated CaF₂ powder from Kletno.

Fig. 7 Temperature dependence of (A) lifetimes τ_1 , τ_2 of exponential components resolved in positron-lifetime spectrum, (B) the relative intensity I_1 of the shorter component. Results measured on naturally irradiated CaF₂ powder from Kletno are

1
2
3 plotted by circles, while squares show results for the reference non-irradiated CaF₂
4 powder. Position of the bulk CaF₂ lifetime is indicated by the dashed line in the upper
5 panel. The inset presents zoomed temperature dependence of the lifetime τ_1 .
6
7
8
9

10 **Fig. 8** Experimental Doppler broadened annihilation profiles for non-irradiated CaF₂
11 powder and well-annealed pure Mg reference sample compared with calculated HMP
12 curves for perfect Mg and CaF₂ crystal. Solid and dashed lines show the HMP curves
13 calculated using GGA and LDA approach, respectively.
14
15
16
17
18

19 **Fig. 9** The calculated HMP curve for a perfect CaF₂ crystal with contributions of
20 various core electron orbitals shown. The HMP curve was calculated using GGA
21 approach. The partial contributions of Ca- and F-electrons are plotted by solid and
22 dashed lines, respectively. Total contributions of positrons annihilated by Ca- and F-
23 electrons are plotted in the figure as well.
24
25
26
27
28
29
30

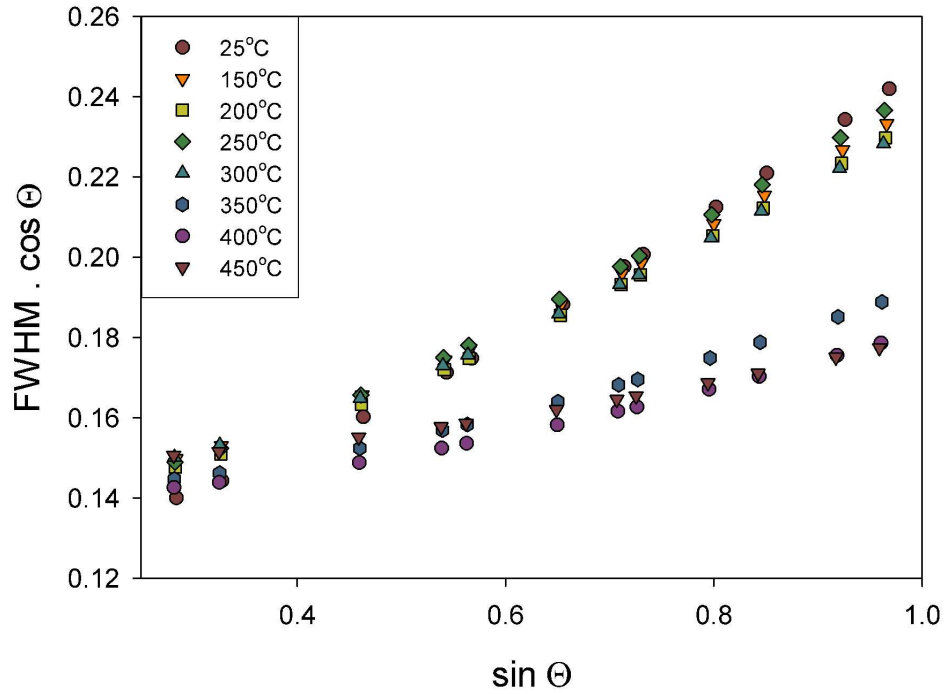
31 **Fig. 10** (A) Experimental CDB ratio curves (related to pure Mg reference sample) for
32 virgin, non-irradiated CaF₂ powder and for naturally irradiated CaF₂ from Kletno. The
33 latter sample was measured in the as-received (irradiated) state and after annealing up
34 to various temperatures. (B) A detail of the amplitude of the peak in CDB ratio curves
35 located at momentum $p \approx (9 \times 10^{-3}) m_0c$.
36
37
38
39
40
41
42

43 **Fig. 11** Calculated ratio curves (related to pure Mg) for free positrons annihilating in a
44 perfect CaF₂ crystal (bulk) and positrons trapped at Ca-vacancy (V_{Ca}), agglomerate of
45 4 F-vacancies (V_{F4}), and agglomerate of 8 F-vacancies (V_{F8}). The ratio curves were
46 calculated using GGA approach.
47
48
49
50
51
52

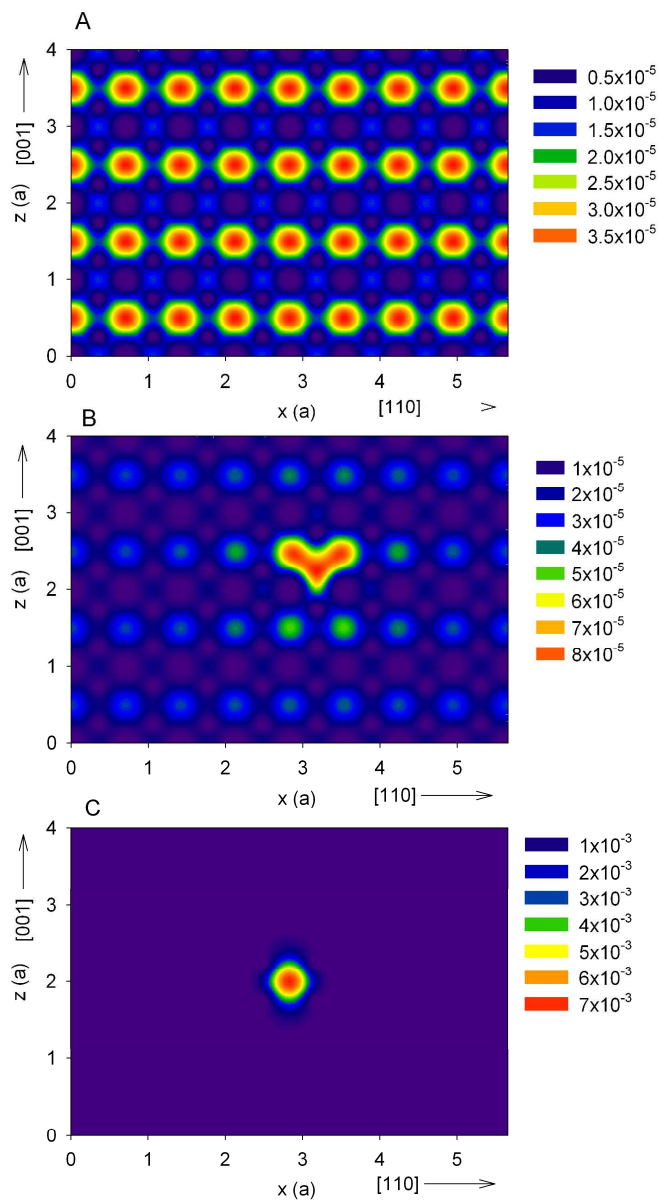
53 **Fig. 12** Photoluminescence spectra of long-time irradiated CaF₂ untreated (A) and
54 after annealing up to 450 °C (B).
55
56
57
58
59
60

1
2
3 **Fig. 13** Weak-beam dark-field TEM images with $g = 022$ of low-irradiated sample
4 from Vlastějovice showing dislocation loops (A) and high-irradiated sample from
5 Kletno displays extreme dislocation density (B).
6
7
8
9

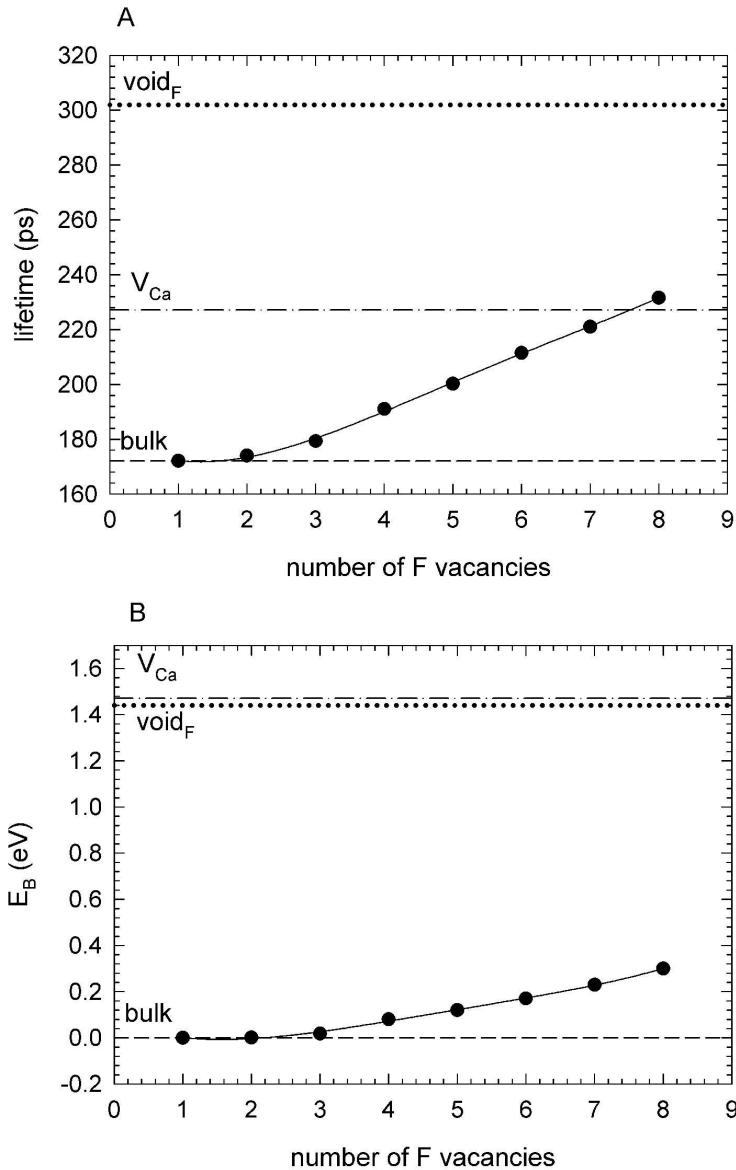
10 **Fig. 14** HRTEM images of high-irradiated sample from Kletno (left) and detail of
11 clustered F -centres, indicated by the arrow (right). Inset in the left image is a Fast
12 Fourier Transform image from the squared area, which corresponding to the right
13 image.
14
15
16
17
18
19
20
21
22
23
24
25
26
27
28
29
30
31
32
33
34
35
36
37
38
39
40
41
42
43
44
45
46
47
48
49
50
51
52
53
54
55
56
57
58
59
60



Williamson-Hall plot showing the data obtained through whole powder pattern fitting. The source powder patterns were measured in-situ during annealing. The micro-strain is proportional to the slope of the linear regression.
631x486mm (150 x 150 DPI)

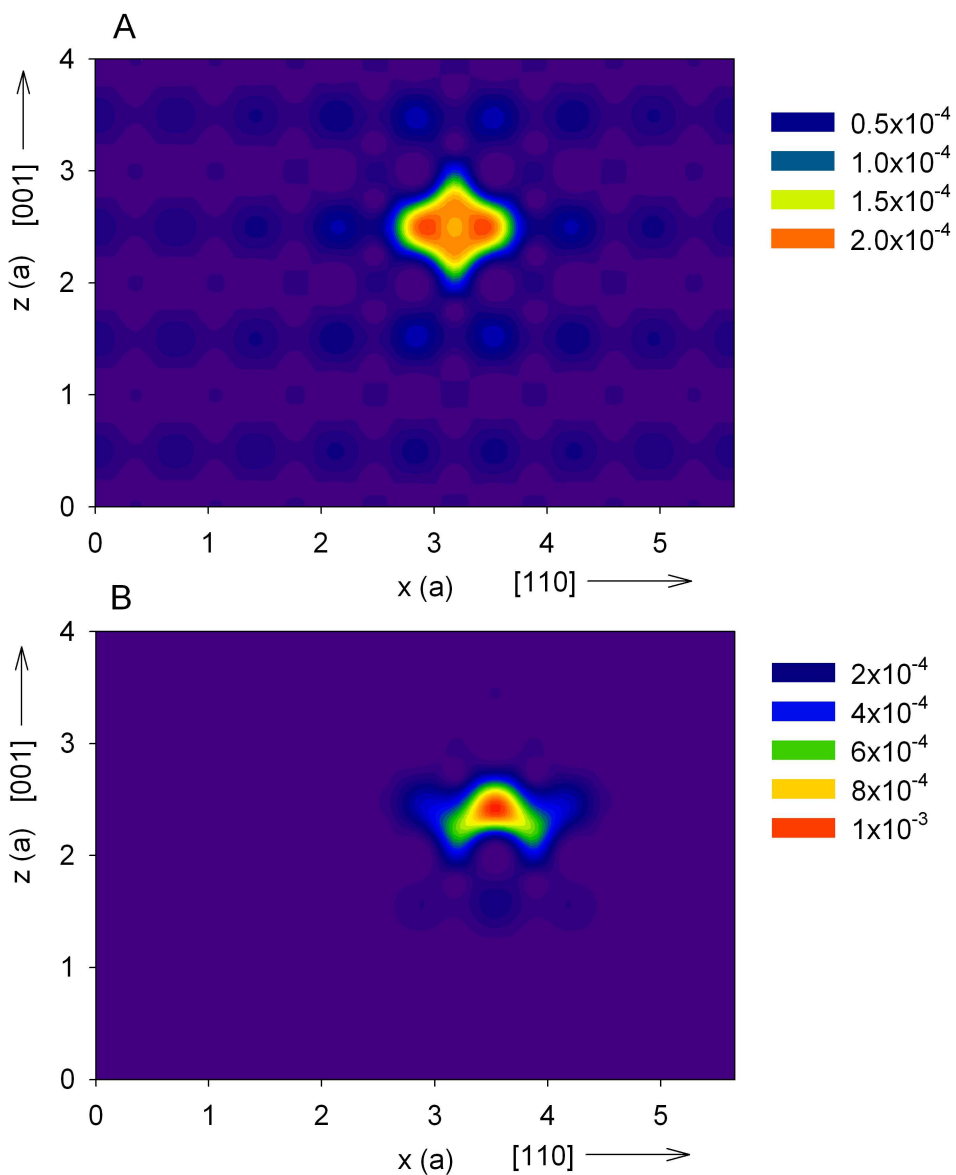


Calculated positron density in (110) plane for (A) a perfect CaF₂ crystal, (B) CaF₂ crystal containing F-vacancy, and (C) CaF₂ crystal containing Ca-vacancy. Positron density is expressed in atomic units; distances are shown in units of CaF₂ lattice parameter.
499x877mm (150 x 150 DPI)



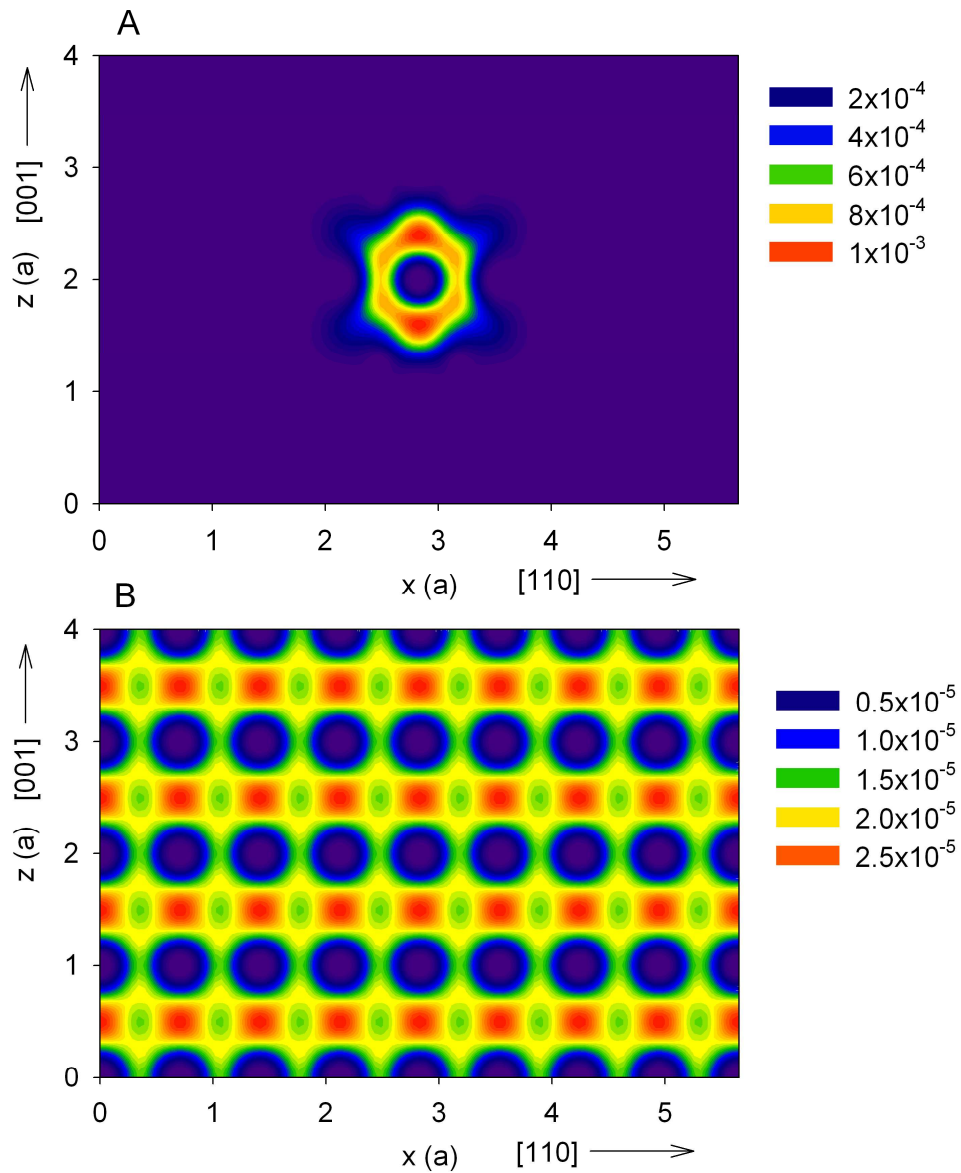
Results of first principle calculations of positron parameters for F-vacancy agglomerates: (A) positron lifetime and (B) positron binding energy as a function of number of F-vacancies in the agglomerate. Dashed lines show positron parameters for a perfect CaF₂ crystal, dash-dotted lines show positron parameters for Ca-vacancy and dotted lines show positron parameters for a large fluorine void.

501x778mm (150 x 150 DPI)

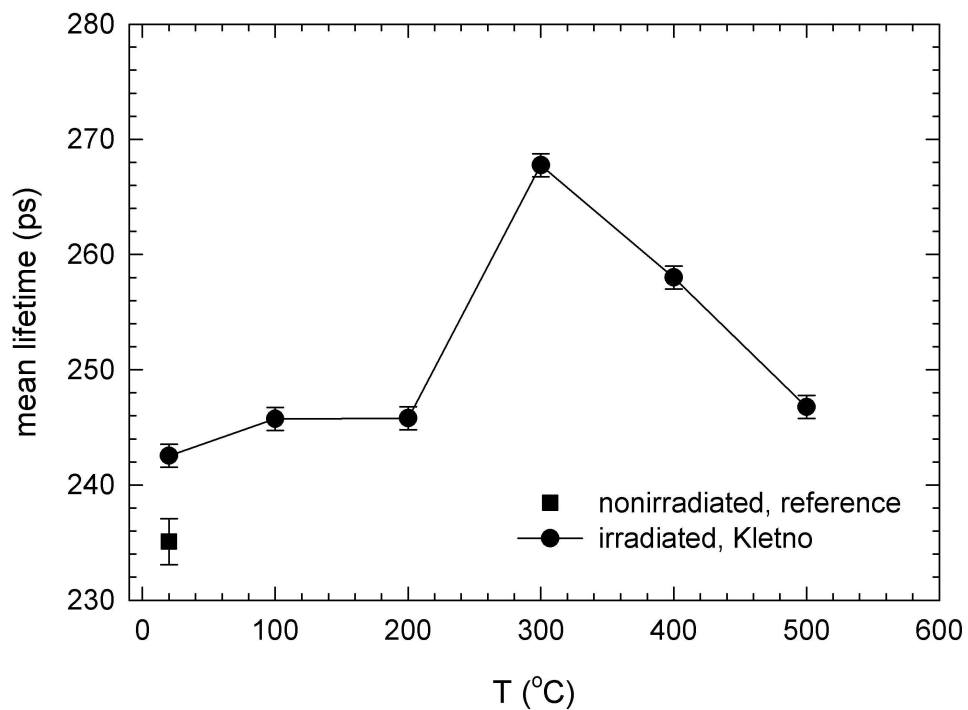


Calculated positron density in (110) plane for a CaF₂ crystal containing (A) F-divacancy, (B) F-tetravacancy. Positron density is expressed in atomic units; distances are shown in units of CaF₂ lattice parameter.

500x594mm (150 x 150 DPI)

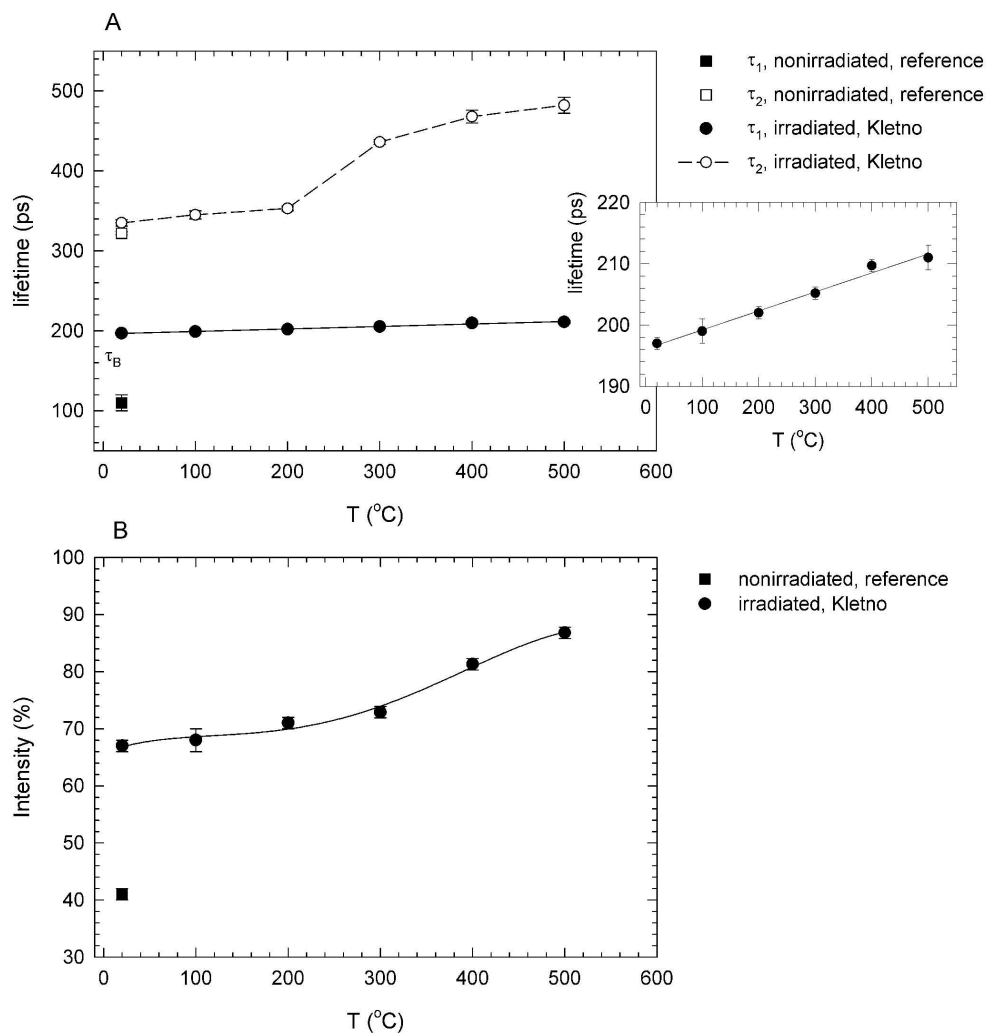


Calculated positron density in (110) plane for a CaF₂ crystal containing (A) an agglomerate of 8 F-vacancies, (B) a large fluorine void. Positron density is expressed in atomic units; distances are shown in units of CaF₂ lattice parameter.
501x594mm (150 x 150 DPI)



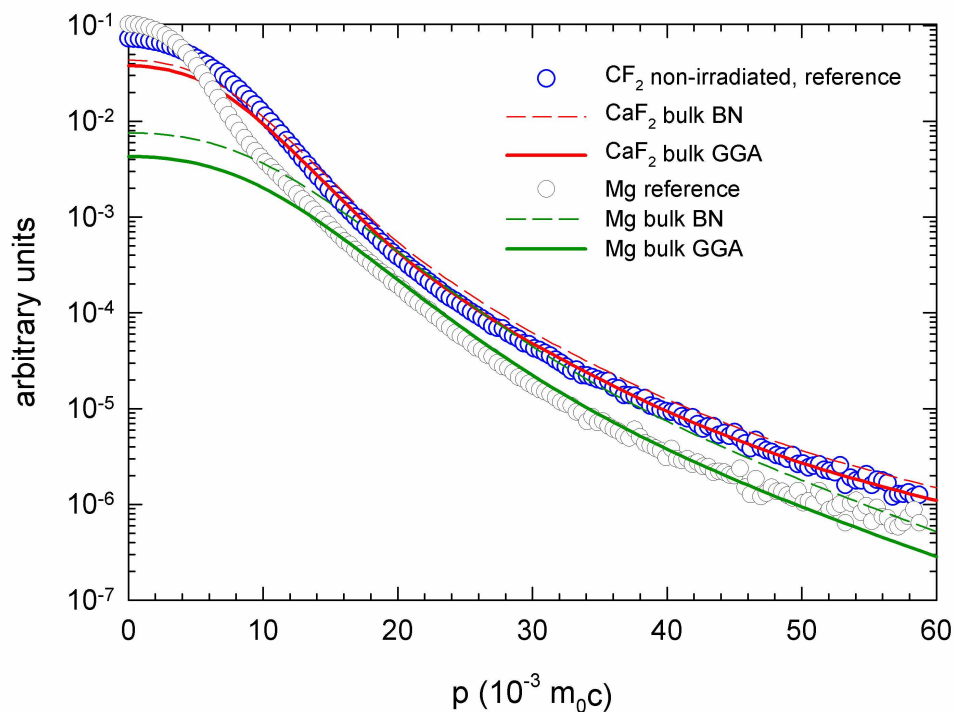
Temperature dependence of the mean positron lifetime τ_{mean} for naturally irradiated CaF₂ powder from Kletno.

493x397mm (150 x 150 DPI)



Temperature dependence of (A) lifetimes τ_1 , τ_2 of exponential components resolved in positron-lifetime spectrum, (B) the relative intensity I_1 of the shorter component. Results measured on naturally irradiated CaF₂ powder from Kletno are plotted by circles, while squares show results for the reference non-irradiated CaF₂ powder. Position of the bulk CaF₂ lifetime is indicated by the dashed line in the upper panel. The inset presents zoomed temperature dependence of the lifetime τ_1 .

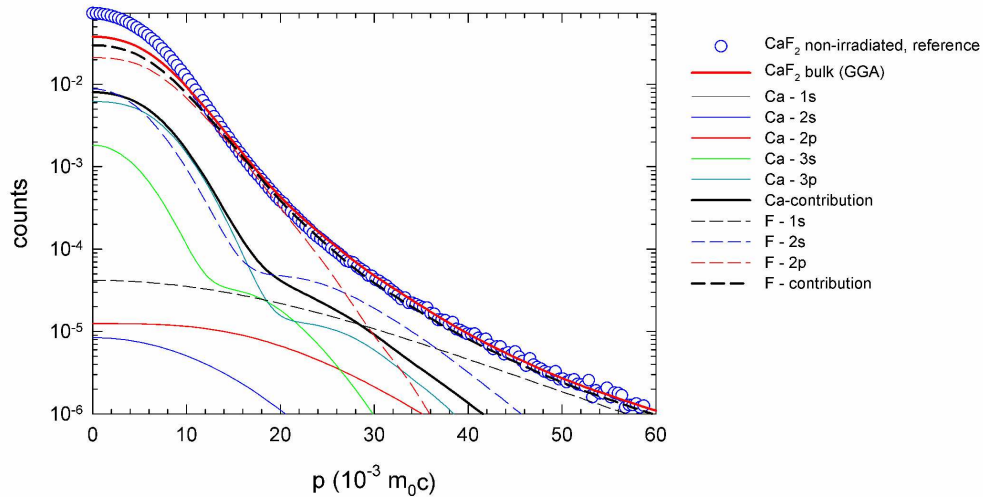
711x757mm (150 x 150 DPI)



Experimental Doppler broadened annihilation profiles for non-irradiated CaF_2 powder and well-annealed pure Mg reference sample compared with calculated HMP curves for perfect Mg and CaF_2 crystal. Solid and dashed lines show the HMP curves calculated using GGA and LDA approach, respectively.

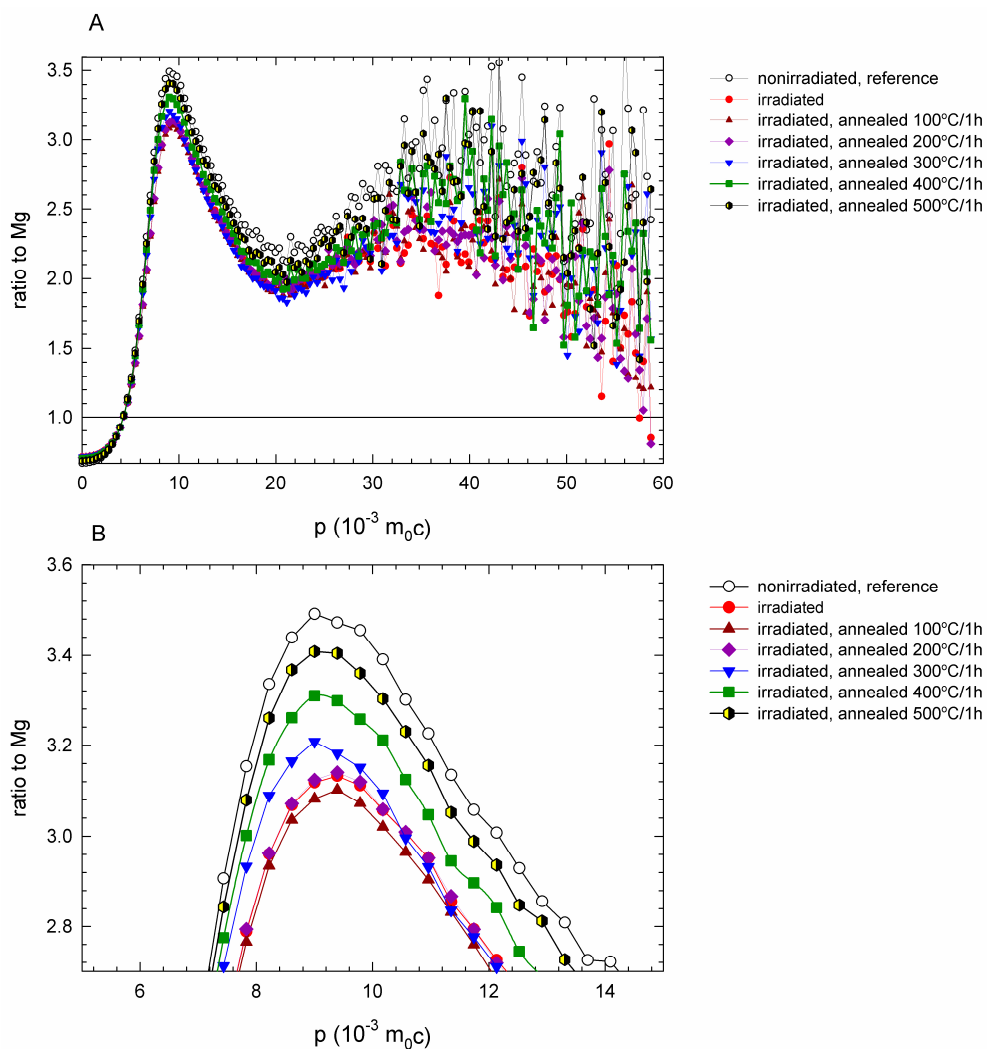
494x402mm (150 x 150 DPI)

Only

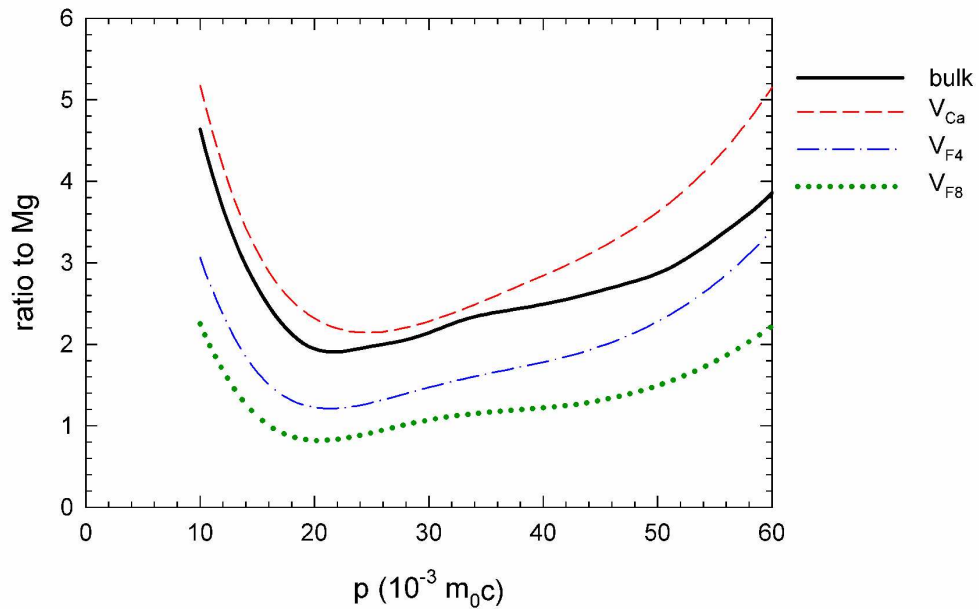


The calculated HMP curve for a perfect CaF₂ crystal with contributions of various core electron orbitals shown. The HMP curve was calculated using GGA approach. The partial contributions of Ca- and F-electrons are plotted by solid and dashed lines, respectively. Total contributions of positrons annihilated by Ca- and F-electrons are plotted in the figure as well.

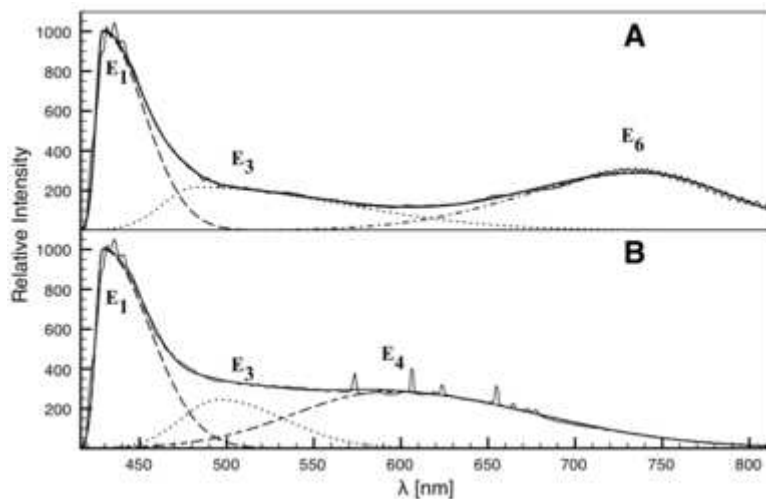
710x384mm (150 x 150 DPI)



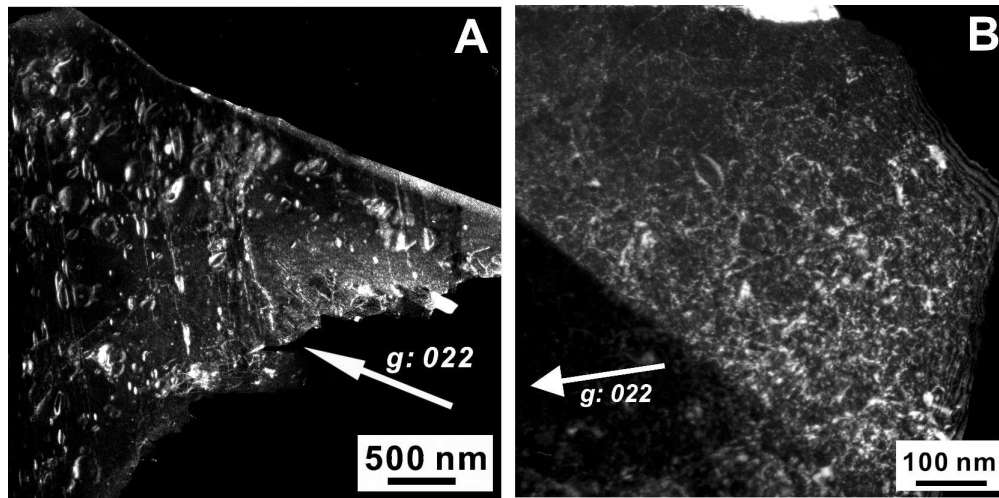
(A) Experimental CDB ratio curves (related to pure Mg reference sample) for virgin, non-irradiated CaF₂ powder and for naturally irradiated CaF₂ from Kletno. The latter sample was measured in the as-received (irradiated) state and after annealing up to various temperatures. (B) A detail of the amplitude of the peak in CDB ratio curves located at momentum $p \approx (9 \times 10^{-3}) m_0c$.
751x789mm (150 x 150 DPI)



Calculated ratio curves (related to pure Mg) for free positrons annihilating in a perfect CaF₂ crystal (bulk) and positrons trapped at Ca-vacancy (VCa), agglomerate of 4 F-vacancies (VF₄), and agglomerate of 8 F-vacancies (VF₈). The ratio curves were calculated using GGA approach.
581x405mm (150 x 150 DPI)

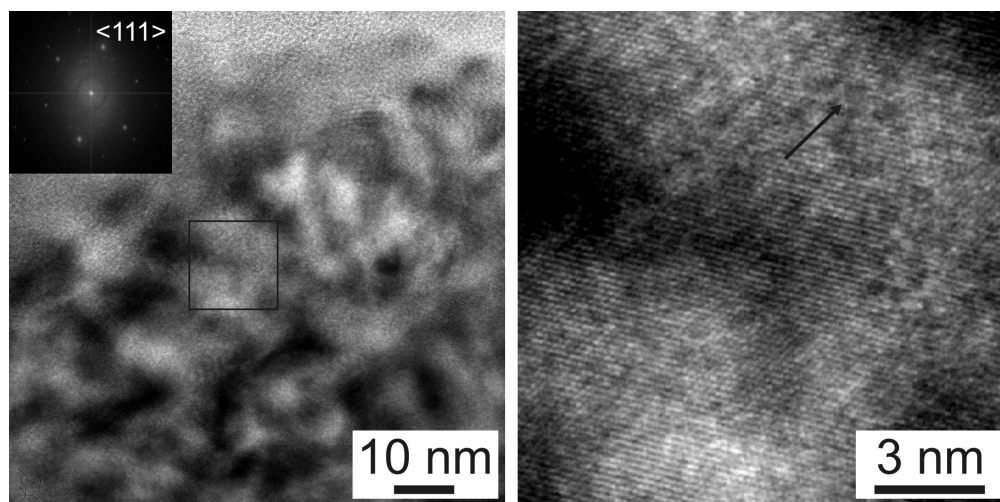


Photoluminescence spectra of long-time irradiated CaF₂ untreated (A) and after annealing up to 450 °C (B).
16x10mm (600 x 600 DPI)



Weak-beam dark-field TEM images with $g = 022$ of low-irradiated sample from Vlastějovice showing dislocation loops (A) and high-irradiated sample from Kletno displays extreme dislocation density (B).

169x83mm (500 x 500 DPI)



HRTEM images of high-irradiated sample from Kletno (left) and detail of clustered F-centres, indicated by the arrow (right). Inset in the left image is a Fast Fourier Transform image from the squared area, which corresponding to the right image.
100x49mm (600 x 600 DPI)